coatings

Article

Influence of Plasma Arc Current and Gas Flow on the Structural and Tribological Properties of TiN Coatings Obtained by Plasma Spraying

Aidar Kengesbekov

PlasmaScience LLP, Ust-Kamenogorsk 070000, Kazakhstan; kenesbekovaidar@gmail.com; Tel.: +7-777-245-2066

Abstract: This study investigates the development of TiN-based coatings using plasma spraying technology, focusing on how plasma arc current and working gas flow rate affect the coatings' structural-phase composition and mechanical–tribological properties. The research highlights the potential and effectiveness of plasma spraying for TiN coatings. Results from scanning electron microscopy and nanoindentation tests show that the TiN coatings have a dense microstructure with strong adhesion. Tribological testing demonstrated that coatings deposited at a 250 A arc current displayed the lowest coefficient of dry friction and the lowest porosity (2.13%) compared to those deposited at 350 A and 450 A arc currents, which exhibited higher porosity (up to 10.45%).

Keywords: coatings; plasma spraying; titanium nitride; wear resistance; microhardness

check for updates

Citation: Kengesbekov, A. Influence of Plasma Arc Current and Gas Flow on the Structural and Tribological Properties of TiN Coatings Obtained by Plasma Spraying. *Coatings* **2024**, *14*, 1404. https://doi.org/10.3390/coatings14111404

Academic Editors: Peihu Gao, Qiaoqin Guo, Yazhe Xing and Yongchun Guo

Received: 9 October 2024
Revised: 1 November 2024
Accepted: 1 November 2024
Published: 5 November 2024

1. Introduction

The increased interest shown by researchers in the last ten years to TiN coatings is related to the prospects of their practical application, as they successfully combine high hardness with wear resistance and chemical stability [1]. Titanium nitride coatings are quite universal in relation to the materials to be processed. They are successfully used in conditions of predominantly abrasive wear in the processing of most materials, including structural steels, cast irons, bronzes, etc. Their efficiency is much lower when cutting ductile chromium–nickel steels, titanium and titanium alloys, and aluminum. TiN coating is used on all types of tools (metal cutting tools, punches, dies, etc.), where heating of the cutting edge up to the temperature of 400–500 °C is allowed [2–4]. TiN coatings, in addition to wear resistance and corrosion resistance, have a number of other important characteristics, including optical and electronic [5–9]. For example, the possibilities of using such coatings in microelectronics to create diffusion barriers in semiconductor devices and in optics as wavelength-selective transmission films have been noted [10–13].

The method chosen for applying TiN (titanium nitride) coatings is influenced by factors such as the geometry and design of the parts to be coated, their technological characteristics, operating conditions, and the desired thickness of the protective layer. The research highlighted in [14,15] examined how different technological parameters affect the resistance of steel surfaces to pitting corrosion when TiN coatings are applied using ion-plasma techniques. It was discovered that, under optimal coating conditions, the corrosion resistance of steel could be enhanced by up to ten times.

The following methods of TiN coatings' deposition are the most widespread in the industry today: magnetron sputtering, PVD/CVD (Physical Vapor Deposition/Chemical Vapor Deposition) spraying, and reactive plasma spraying [16–18]. The only factor uniting all available methods is the thermal effect during the application of the protective layer, which is necessary for the formation of a stable adhesive bond between the coating and the substrate. Each of the above methods has its own advantages and disadvantages that determine its effective field of application [19]. Moreover, their application is also limited by energy problems arising during heating of large-sized parts since the required density and adhesion are achieved by subsequent heat treatment of the formed layer. Therefore, one of the most economical and easy-to-implement methods of TiN coating is the plasma spraying method, which allows forming and melting the layer in one operation.

Plasma spraying (PS) is a promising process for the deposition of nitride coatings. However, to the best of our knowledge, few studies have been conducted on the production of oxide-free TiN coatings by the PS method. Based on the literature analysis, it can be argued that further development of PS has great potential for sputtering nitride coatings.

To avoid contamination, proper protection of particles and sludge by inert gas during sputtering is necessary. To date, the most reliable method is the use of a special vacuum chamber. However, this type of equipment is expensive and limits the size of the part to be treated. One of the solutions to these problems is the use of a "shield cover" in the design of the plasmatron. The present work offers a simpler way of solving this problem.

The proposal involves the use of a special plasmatron, which is equipped with additional channels for powder and nitrogen supply. These features of the plasmatron ensure the formation of nitrides due to the reaction of nitrogen with metal powders as well as the formation of a nitrogen envelope around the plasma jet, which prevents significant oxidation of powders and coatings. This method is simple and versatile, allowing for the machining of large size and complex configuration parts.

The author of this work is confident that by refining the system and selecting the modes of PS, wear-resistant nitride coatings with low oxide content can be obtained [20–30].

The purpose of the present work is to understand the relationship between the phase composition, microstructure, mechanical and tribological properties of titanium nitride coatings obtained by plasma spraying methods

Special attention is paid to the tribological properties, and the wear mechanism is analyzed. It is hoped that this study may provide some useful information on the design and application of titanium nitride coatings as wear-resistant coatings.

2. Materials and Methods

The substrate material used was AISI 304 (1.4301) steel. To enhance the adhesion between the coating and the substrate, the flat surface of a 60 mm × 40 mm × 4 mm steel sample was cleaned with acetone and sandblasted before coating. TiN powders with a particle size of 15–40 µm were used for the coating process. The experiment employed an plasma spraying system, where the substrate was preheated to 250 °C using a plasma jet, with the temperature monitored by an NT-819 pyrometer. The TiN coatings were applied to the preheated substrate using a plasma torch. The surface morphology of the coatings was analyzed using scanning electron microscope JEOL JSM 6390 (Tokyo, Japan) is used with an attachment for element analysis (EDS, Tokyo, Japan).

The phase composition of the samples under investigation was analyzed using a Philips X'pertpro (Almelo, The Netherland) X-ray diffractometer, employing CuKα X-ray radiation. The imaging was performed under the following conditions: tube voltage set to 40 kV, tube current at 30 mA, exposure time of 1 s, and a scanning step size of 0.02°. The study of phase composition and structural parameters of the samples was carried out on a diffractometer XRD-6000 on Cu Kα-radiation. The analysis of the phase composition was carried out using PDF 4+ databases and the POWDER CELL 2.4 full-profile analysis program.

Wear resistance was evaluated using a high-temperature tribometer TRB^3 (Anton Paar, Graz, Austria) with the "ball-on-disk" method, as per international standard ASTM G99 [31]. The counterbody was a 6.0 mm diameter ball made from Si_3N_4-coated steel. The tests were conducted with a load of 6 N, a linear velocity of 3 cm/s, a wear radius of a curvature of 4 mm, and a friction path of 100 m. The wear track left by the ball after 1000 revolutions was captured using a non-contact profilometer, Micro Measure 3D Station (Marposs, Bentivoglio, Italy). From this, track areas were measured at six different points to calculate an average value. Surface roughness was assessed using a profilometer from the Proton plant, model 130, following the standard method (GOST-2789-73). The mechanical properties of the coatings, including Young's modulus and hardness, were tested using a NanoScan-4DCompact nano-hardness tester. Testing involved a load of 50 mN with a loading time of 10 s, an unloading time of 10 s, and a maximum load maintenance time of 2 s. The relationship between penetration depth and applied force during loading and unloading was determined using the Oliver–Farr method.

Friction and wear testing was conducted using a reciprocating motion scheme at room temperature in air, following ASTM G133 standards (Figure 1) [32]. These tests were carried out on equipment developed at Wroclaw University of Science and Technology [33]. The method involved measuring the friction force with a strain gauge as test samples, which were of known shape and pressed together with a specified force, moved relative to each other. The coefficient of friction was calculated directly during testing as the ratio of the measured friction force to the applied pressing force. The tests were performed with a load ranging from 9.22 to 10.42 N and an average sliding velocity of 0.072 m/s. The working stroke length was 14.4 m, and the test duration was 200 s. Friction force was continuously recorded, and fractographic analysis of wear patterns was conducted using an optical microscope to assess the abrasion by examining wear grooves on the sample.

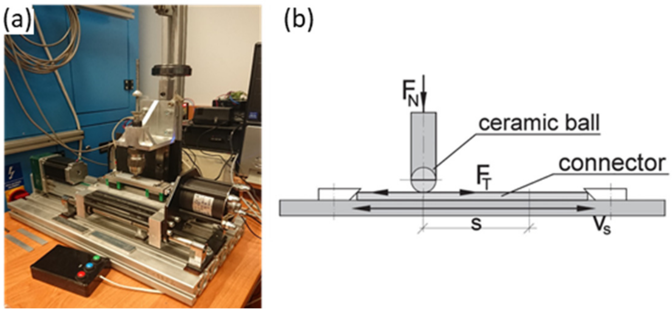

Figure 1. Test rig with reciprocating motion: (**a**) installation for testing according to ASTM G133; (**b**) scheme of the "ball-and-plate" method [32].

Abrasive wear tests on the samples were conducted using a specialized experimental setup following GOST 23.208-79, using a "rotating roller–flat surface" configuration [34] (Figure 2a). Prior to testing, the sample surfaces were ground, polished, cleaned with acetone, and dried. A cylindrical rubber roller, pressed with a force of 22 N against the flat surface of the test sample, was rotated at one rotation per second. Abrasive particles were fed at a rate of 41–42 g/min between the rubber wheel and the sample, with an electrocorundum of 200–250 µm grain size used as the abrasive material. The wear resistance of the treated samples was assessed by comparing their wear to that of a reference (untreated) sample. Wear was measured using ADV-200 analytical scales (KERN & SOHN GmbH, Ebingen, Germany) with a precision of 0.0001 g. The samples were weighed every minute over a three-minute test period, resulting in a total wear distance of 28.8 mm. To ensure accurate measurements, samples were blown with compressed air to remove any residual sand particles before weighing. The wear resistance was evaluated based on the mass loss of the samples during testing, in accordance with GOST 23.208-79.

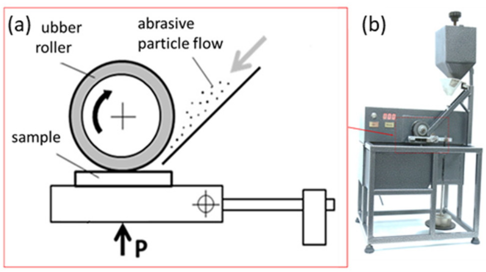

Figure 2. Experimental stand for testing samples: (**a**) abrasive wear according to the scheme "rotating roller–flat surface" in accordance with GOST-23.208-79; (**b**) abrasive wear test set-up [34].

3. Results and Discussion

Titanium nitride (TiN) powder was selected as an object of study for coating. A study of the surface of TiN powder particles by electron microscopy methods showed that the particles have an angular shape of size from 15 to 45 microns with a smooth surface and light gray color; the chemical composition of the powder is shown in Figure 3. Figure 3b shows the diffractogram of TiN powder. According to the results of the data presented, it was found that the main phases in the powder are titanium nitride and a small content of titanium oxide.

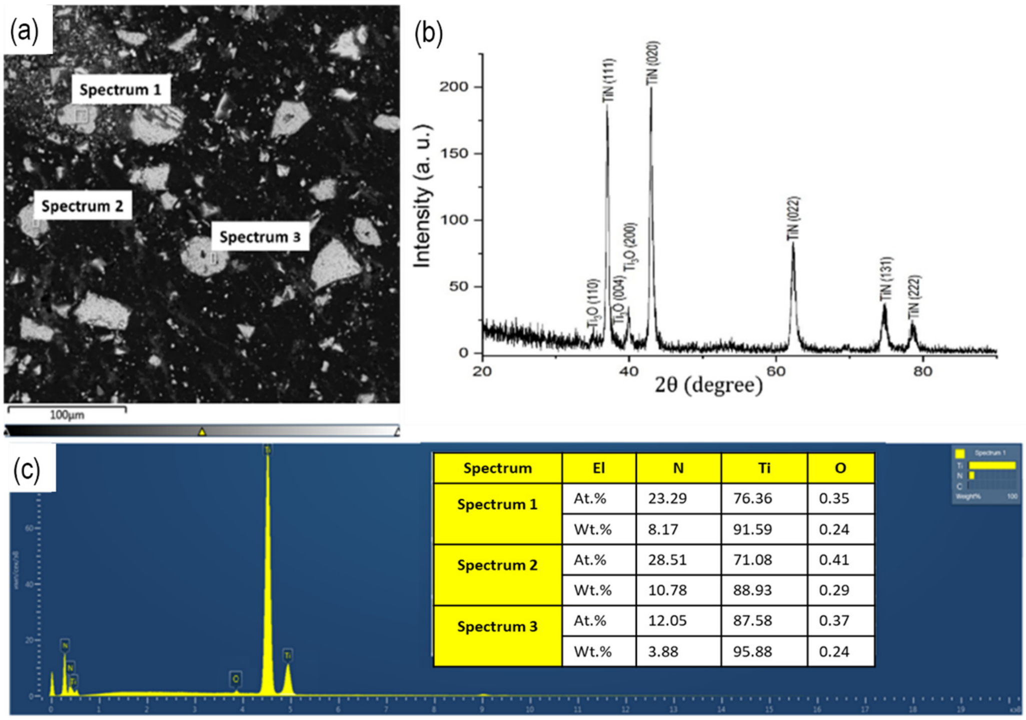

Figure 3. Structure-phase states of titanium nitride powder: (**a**) SEM image of the powder, (**b**) powder diffraction, and (**c**) powder chemistry.

The quality of coatings applied via air-plasma spraying is influenced by several factors, including spraying distance, current, voltage, and gas pressure. Among these, the strength of the electric current and the pressure of the working gas (Ar) are particularly significant. The range of plasma-gas flow rates is connected to the operational conditions of the plasma torch, such as thermal load on the nozzle walls, anode resistance, and process stability. To determine the plasma-gas flow rate, the technical conditions were adjusted, with variable arc currents ranging from 250 to 450 A, and the flow rate was monitored based on plasma combustion stability. Consequently, specific spraying parameters were chosen for the deposition process (Table 1).

Table 1. Regimes of air-plasma spraying of TiN coatings.

Sample	TiN(34_250)	TiN(37_350)	TiN(40_450)
Ar gas flow rate, L/min	34	37	40
Current, A	250	350	450
Spraying distance, mm	150	150	150
Gas flow rate N, bar	3	3	3
Processing time, s	60	60	60

3.1. Microstructure

Figure 4 displays the diffractograms of TiN coatings applied to the surface of AISI 304 (1.4301) steel under various PS conditions. The coatings were primarily composed of TiN (PDF4+ database references: 96-101-1101), with a minor presence of Ti_2O_3 (PDF4+ database references: 96-110-1044). The diffractogram revealed five prominent TiN peaks corresponding to the diffraction planes (111), (200), (220), (131), and (222), which are characteristic of the FCC phase structure. The diffraction peaks for Ti_2O_3, including (012), (110), (024), (113), (024), (116), and (300), exhibited relatively low intensities. The XRD analysis of the three samples showed a gradual decrease in the TiN phase content and a corresponding increase in the Ti_2O_3 oxide phase moving from Sample (a) to Sample (c). This trend is evident from the changes in peak intensities and relative proportions depicted in the pie charts, indicating that Sample (a) has the highest TiN content and lowest oxide content, while Sample (c) has the highest Ti_2O_3 content. The observed differences in phase composition suggest variations in processing conditions or potential oxidation effects during sample preparation, leading to increased formation of the oxide phase in Sample (c).

Research conducted by Ma H. et al. (2024) [35] and Zheng Q. et al. (2023) [36] supports the assertion that TiN coatings frequently form Ti_2O_3 as a secondary phase when subjected to high temperatures or oxidative environments. The present author's observations regarding the relationship between processing conditions and oxide formation align with these conclusions, emphasizing the need for careful control of deposition conditions to minimize undesirable oxidation. Conversely, some studies, such as those by Fan X. et al. (2022) [37], have suggested that certain levels of Ti_2O_3 could be beneficial, potentially enhancing the wear resistance of the coatings. In the present study, although an increased presence of oxides was observed, which may contribute to potential brittleness, it is acknowledged that the role of Ti_2O_3 may be multifaceted. This complexity underscores the necessity for further investigation into its impact on the mechanical properties of the coatings.

The analysis of three different TiN samples revealed variations in phase composition, crystallite size, and lattice distortions, which significantly affect the material's properties. Sample TiN(34_250) has the highest TiN content (89%) and the largest crystallite size (44 nm), which, combined with its highest lattice distortion (2.5×10^{-3}), indicates increased hardness but also greater internal strain and potential brittleness. Sample TiN(37_350) shows a balanced phase composition, lower crystallite size (35 nm), and reduced lattice distortion (0.6×10^{-3}), making it more structurally stable with less strain. Sample TiN(40_450) is similar to Sample 2 in crystallite size and lattice distortion but has a slightly higher Ti_2O_3 content (10%), suggesting slightly increased internal stress and potential oxidation susceptibility.

The relationship between crystallite size, lattice distortion, and mechanical properties is well documented. Research conducted by Mittemeijer and Welzel (2008) [38] emphasized that larger crystallite sizes can lead to increased hardness, whereas higher lattice distortions may contribute to internal strain, potentially resulting in brittleness. The results of the present author's observations support these findings, particularly in relation to Sample 34_250.

The microstructural analysis of the coatings presented in Figure 5 reveals a lamellar structure typical of thermal spray techniques, with a consistent coating thickness of approximately 60–100 μm. The SEM analysis showed a heterogeneous structure due to uneven heating of powder particles in the plasma jet, resulting in some weakly deformed particles and internal cracks. These cracks are attributed to insufficient heating, causing thermal stress, either from the remelting of the powder or differences in thermal expansion between the particles and the substrate.

One of the main quality indicators of wear-resistant functional coating is its porosity. The porosity of titanium nitride coatings obtained using plasma spraying has been studied. The characteristics of pore location, their typical sizes, and the influence of some technology parameters on the process of porosity formation in these coatings have been established

(Figure 5). The microstructure of TiN(34_250) coating is characterized by relatively high density (compared to TiN(37_350), TiN(40_450)) and low porosity, without destruction of connections at the coating–substrate boundary, as shown in Figure 5a. The volume fraction of pores is 2.13% of the coating surface area. There are also pores with smaller size, formed as a result of degassing of molten material of particles during their crystallization.

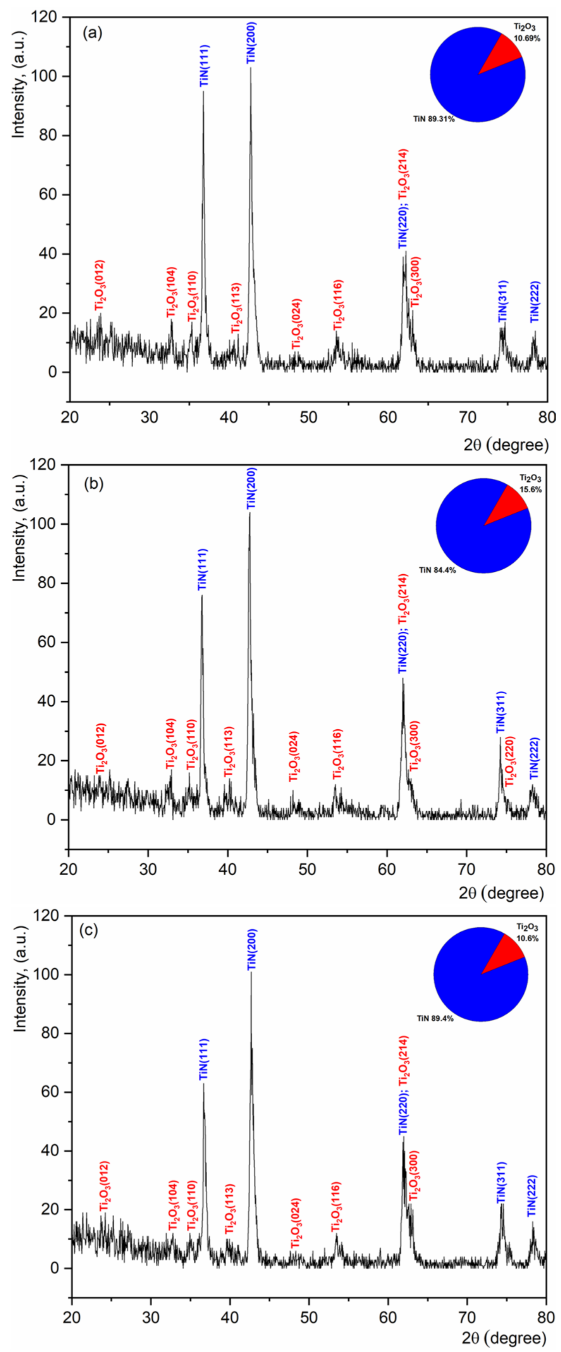

Figure 4. Diffractograms of TiN coatings: (**a**) TiN(34_250); (**b**) TiN(37_350); (**c**) TiN(40_450).

Figure 5b,c shows the microstructure of TiN(37_350) and TiN(40_450) coatings, which is characterized by the presence of porosity throughout the thickness of the coatings. The coating area at the boundary with the substrate is characterized by a more uniform structure with no delamination at the coating–substrate boundary. The pores showed irregular shape and sizes up to 10 µm. The porosity of TiN coating was 6.25 % and 10.45 % at thicknesses of 75 µm and 103 µm, respectively. The formation of the coating occurred due to the collision of particles with the surface of the workpiece and their strong deformation, flattening, and splashing. The time variation of the working gas pressure regulates the coating structure, and as its value increases, a microporous structure can be formed, such as in the TiN regime (40_450). It should be noted that the problem of reducing pores and cracks in the PS, as well as improving the structure of coatings, remains an urgent task requiring further research.

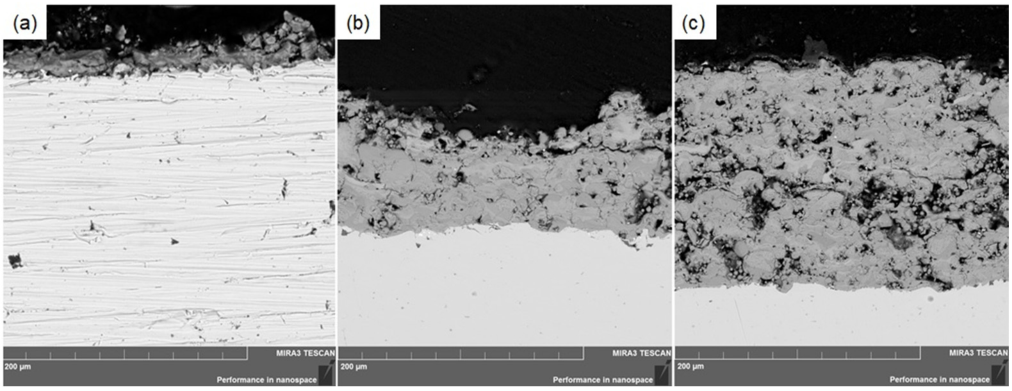

Figure 5. SEM images of cross-sectional structure of TiN coatings: (**a**) TiN(34_250); (**b**) TiN(37_350); (**c**) TiN(40_450).

Figure 6 shows the results of the elemental mapping of the cross-section of TiN coatings. According to the data on the distribution of elements in the surface layer, which were obtained in the mapping mode, the contrast of the composition of TiN coatings is demonstrated.

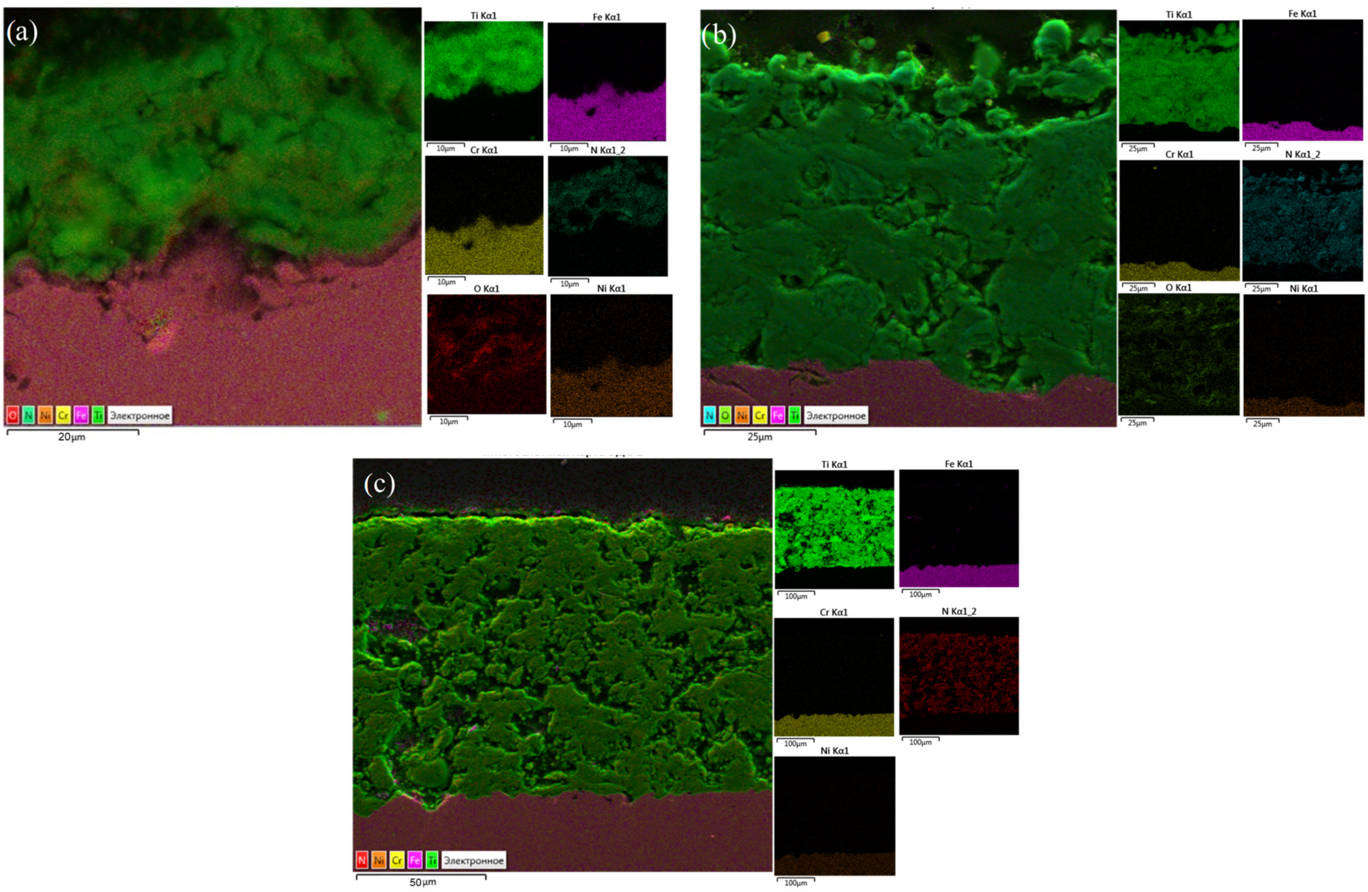

Figure 6. Results of elemental mapping of the cross section of TiN coatings: (**a**) TiN(34_250); (**b**) TiN(37_350); (**c**) TiN(40_450).

According to this, it can be assumed that the predominant phase in this region is TiN. For instance, TiN(34_250) shows a significant presence of nitrogen and titanium, while TiN(37_350) contains small amounts of iron and chromium, and TiN(40_450) has detectable amounts of oxygen and nickel. These compositional differences suggest variations in coating quality and structural integrity across the samples, aligning with the observed microstructural features.

3.2. Properties

3.2.1. Microhardness

On the basis of the results of that mechanical–tribological studies, it was possible to determine the optimum regime of PS for TiN coatings. The TiN(34_250) coating obtained at a current strength of 250 A and working gas (Ar) flow rate of 34 l/min showed better hardness and wear-resistance results relative to TiN(37_350) and TiN(40_450) coatings. Increasing the working gas flow rate reduces the thermal energy for heating the sprayed particles. When the plasma-gas flow rate is higher than the optimum values, the coating density and other indicators of spraying efficiency are significantly reduced. Increasing the operating current leads to an increase in the maximum velocities and temperatures of the particles. However, in this work, the working gas flow rate changed insignificantly. On this basis, the efficiency of the spraying process depended on the operating current, which varied from 250 A to 450 A. For the work regime of the plasmatron at 350 A and 450 A, the powder particles acquired higher velocity and stayed small in the active plasmatron, respectively, and the quality of the obtained coatings decreased. This conclusion was confirmed by the results of SEM images of the structure of the coating cross-section (Figure 5), where coating TiN(34_250) showed a denser and more homogeneous structure compared to coatings TiN(37_350) and TiN(40_450).

The structure study was complemented by microhardness measurements across the entire cross-section of the coating. Figure 7 shows the results of the microhardness measurements of TiN coatings of different regimes. All coatings were generally characterized by high microhardness. Similar results were obtained in [39–41]. No dependence of microhardness on the location of measurement points along the layer height was found. Comparatively high hardness was observed on the surface of the coating processed according to the regime №1, and it has a value of 1250 HV0.1. This is probably due to the low content of pores and cracks on the structure of the TiN(34_250) sample.

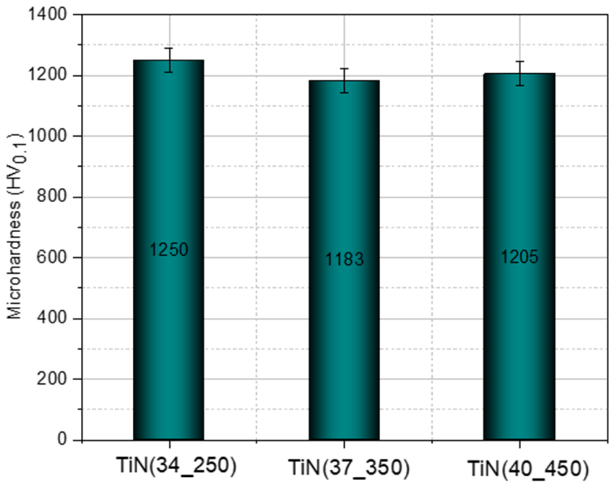

Figure 7. Results of the microhardness of TiN coatings obtained by PS method.

Studies by Khrustalyov A. et al. (2022) [42] and Ghailane A et al. (2022) [43] have documented microhardness values ranging from 1000 to 1400 HV for TiN coatings applied via various plasma spray techniques. A comparative analysis of their processing conditions, including temperature and plasma parameters, demonstrated a significant influence on the resultant hardness values. Notably, the absence of pores and cracks in the coatings produced under regime TiN(34_250) aligns with Zhang's findings, which indicated that denser coatings, achieved through optimized plasma parameters, exhibit enhanced hardness.

3.2.2. Adhesion Test

Adhesion strength is crucial for assessing the effectiveness of coatings. The temperature of the substrate surface significantly affects both the adhesion and cohesion strength of the coatings and their overall structure. Low temperatures, specifically those below 30% of the melting point of the sprayed powder, tend to produce coatings with poor adhesion and cohesion on the treated material's surface. Therefore, prior to applying TiN coatings, the surface of AISI 304 (1.4301) steel was pretreated with plasma at temperatures ranging from 150 to 250 °C, with a plasma treatment distance of 150 mm. The adhesion of the TiN coatings to the substrates was evaluated using the tear-off method.

The results indicate that coating adhesion improves as the surface roughness of the sprayed layer decreases (Figure 8). The TiN(34_250) coating demonstrated superior adhesion compared to the TiN(37_350) and TiN(40_450) coatings. Adhesion strength was assessed using the tear-off method. Examination of the failure modes revealed that, in all cases, the coating tore along the adhesive layer. Consequently, the force required to achieve adhesion to the metal substrate could not be precisely measured. However, since the observed tear force was at least equal to or greater than the adhesive tear force, this type of failure is considered a positive outcome.

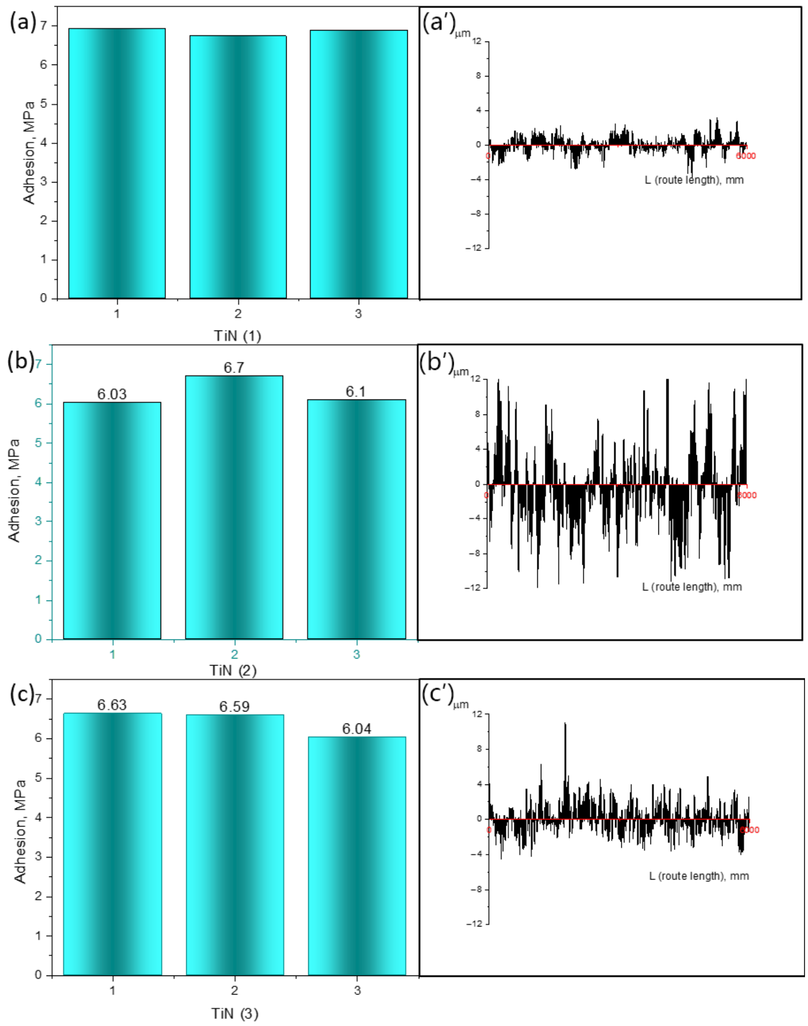

Figure 8. Adhesion strength and roughness of TiN coating: (**a**) TiN(34_250); (**b**) TiN(37_350); (**c**) TiN(40_450); (**a′**) TiN(34_250); (**b′**) TiN(37_350); (**c′**) TiN(40_450).

3.2.3. Nanoindentation

Figure 9 shows the results of hardness and modulus of elasticity measurements of TiN coatings obtained under different spraying regimes. The measurement was carried out on the cross-section of the coatings by nanoindentation method. Hardness is crucial for the plastic deformation resistance of coatings, while elasticity can improve the fracture toughness and strain resistance of coatings. The ratio between hardness (H) and elastic modulus (E) can be defined as the plasticity index (H/E) or the elastic deformation capacity of the material, which can be used to provide the wear behavior of the material [44]. The experimental results showed that the plasticity index (H/E) of the coatings obtained under TiN(34_250), TiN(37_350), and TiN(40_450) regimes are different from each other and have the following values: 0.074, 0.058, and 0.071, respectively. Generally, the larger the H/E value, the better the wear resistance. The findings are consistent with those of Duan L.L. et al. (2023) [45], who reported that an optimal H/E ratio significantly enhances the wear resistance of TiN coatings. Their analysis suggested that coatings with a well-balanced combination of hardness and elasticity can withstand wear more effectively. However, some studies, such as those by Kao W. H et al. (2017) [46], have indicated that merely increasing hardness without a corresponding enhancement in elasticity may not lead to improved wear resistance. This highlights the importance of achieving a balance between these properties rather than solely focusing on maximizing hardness.

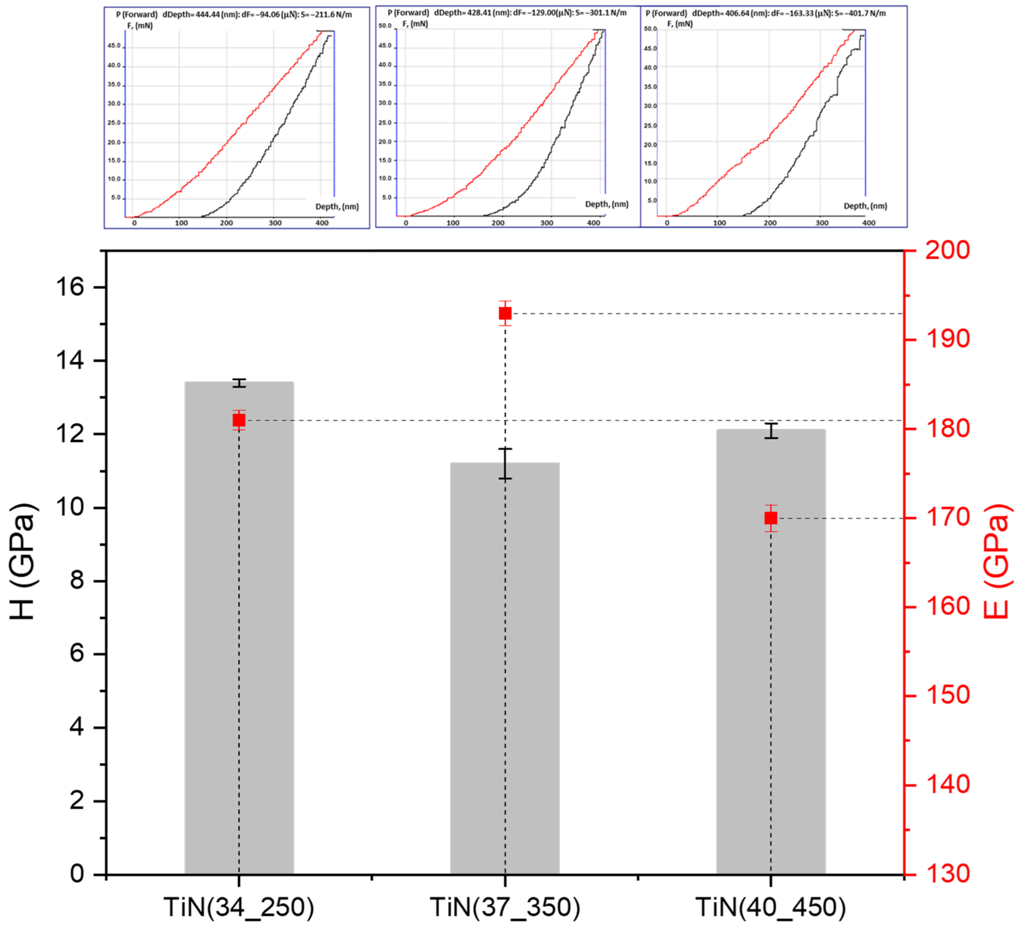

Figure 9. Nanoindentation results of TiN coatings obtained by the PS method.

3.2.4. Tribology

As a result, coatings with higher hardness and lower modulus of elasticity can attenuate interfacial stress and improve anti-wear characteristics [47]. The dependence of the friction coefficient of the investigated samples on the friction path is shown in Figure 10. An analogue curve can be observed for all samples, including a very short period of "run-in"; i.e., the worn surface of coatings and counterbody were adapted to each other and then kept in a stationary mode. It is shown that the coefficient of friction of TiN(34_250) coatings with a counterbody made of Si_3N_4 in dry friction is lower compared to TiN(37_350) and TiN(40_450) coatings, which indicates the relative wear resistance of the coating under the same test conditions.

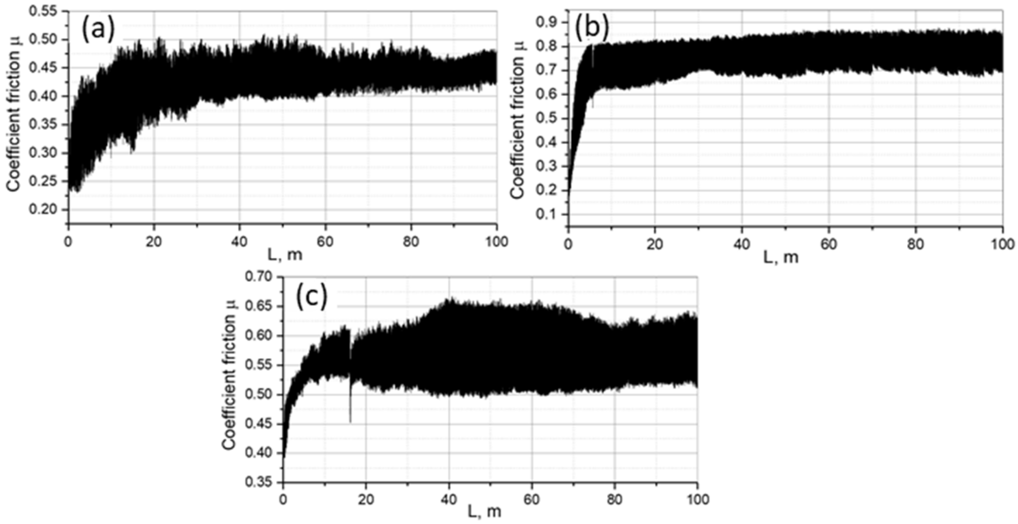

Figure 10. Dependence of the friction coefficient of the coatings on the length of the friction path: (**a**) TiN(34_250); (**b**) TiN(37_350); (**c**) TiN(40_450).

Images of the wear path of the coatings were taken using a 3D profilometer (Figure 11). Upon evaluation of the wear resistance of the samples based on the geometric parameters of the wear paths, it can be said that the width of the wear path of the TiN(34_250) coating sample is significantly smaller compared to that of TiN(37_350) and TiN(40_450). The wear volume proves the improved tribological characteristic of the test specimen with TiN(34_250) coating.

Figure 12 shows the experimental dependences of the coefficient of friction on the number of cycles plotted from the test results for each regime of the sample, respectively. The analysis of the test results showed a weakly increasing coefficient of friction with increasing number of revolutions; that is, all coatings in contact with the contortel, except TiN(34_250), did not withstand tribological tests under the given conditions. The TiN(37_350) and TiN(40_450) samples exhibited very low values at the beginning of the test, which jumped higher after 50 s and 25 s, respectively. The TiN(34_250) sample exhibited a relatively low coefficient of friction, which is stable throughout the friction path. The comparative analysis indicates that the coatings abrade during friction but do not peel off; i.e., they fail by a cohesive mechanism associated with plastic deformation

After the tests, the contact surface of the friction pair of the sample with the counterbody (Al_2O_3 ball) was investigated. Microphotographs of characteristic friction tracks on the surface of the samples are shown in Figure 10a–c. It is necessary to note the different characteristics of the wear of coatings. The analysis of the sizes of friction tracks also allowed to draw a conclusion about the higher wear resistance of TiN(34_250) coating. For TiN(34_250) coatings, the depth of the friction track was 11 μm, and for TiN(37_350) and TiN(40_450) coatings, it was 60 and 50 μm, respectively.

These observations align with research by Zhou Q et al. (2024) [48] and Kara L et al. (2019) [49], which also found that TiN coatings experienced increased friction coefficients over time due to wear mechanisms. Zhou reported that a lack of stability in coefficient of friction during extended tests often correlated with the onset of wear, supporting the present study's conclusions that TiN(34_250) performed more consistently. The notion that coatings fail due to cohesive mechanisms associated with plastic deformation rather than peeling is consistent with findings from studies like those of Duan L. L et al. (2023) [45]. Their work highlighted that lower-quality coatings tend to fail due to delamination, while higher-quality coatings like TiN maintain structural integrity longer due to superior adhesion properties. This stable coefficient of friction for TiN(34_250) could be attributed to its structural characteristics. As pointed out in a study by Tu R et al. (2023) [50], coatings that exhibit a more consistent coefficient of friction often possess a robust microstructure that can better withstand the stresses of friction. In the present study, the results reinforce the notion that optimized deposition conditions have a direct positive impact on tribological performance.

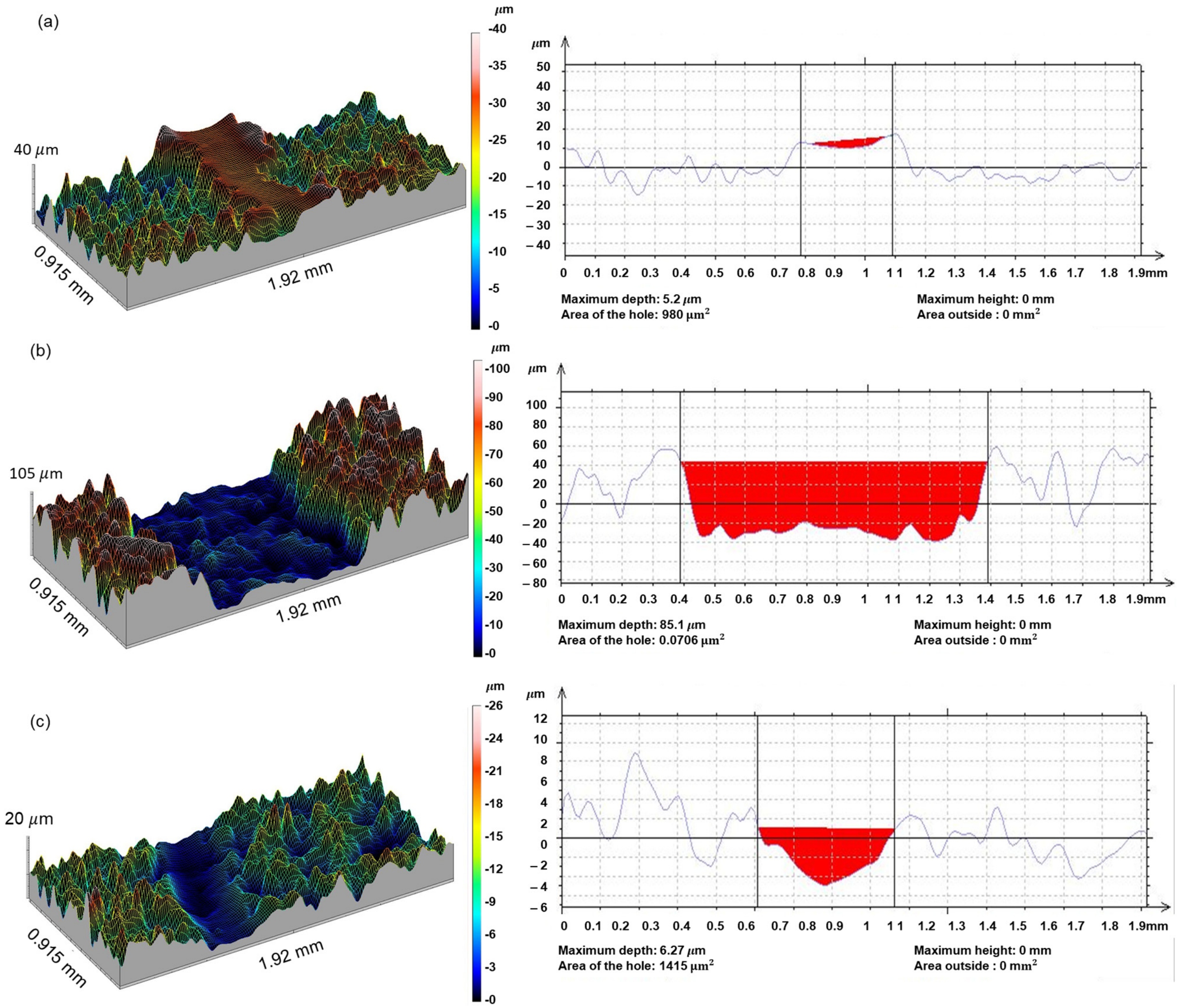

Figure 11. Microphotographs of the contact zone of the counterbody with the coating: (**a**) TiN(34_250); (**b**) TiN(37_350); (**c**)TiN(40_450).

An abrasive wear test was carried out to evaluate the wear resistance of the coatings. The abrasive wear results in terms of loss for the coatings are shown in Figure 13. It can be seen that there was a slight difference in the resistance against abrasion of the samples. The best material among all the studied coatings is TiN(34_250), which showed about 83–87 % higher abrasion resistance compared to the coatings obtained by TiN(37_350) and TiN(40_450) regimes.

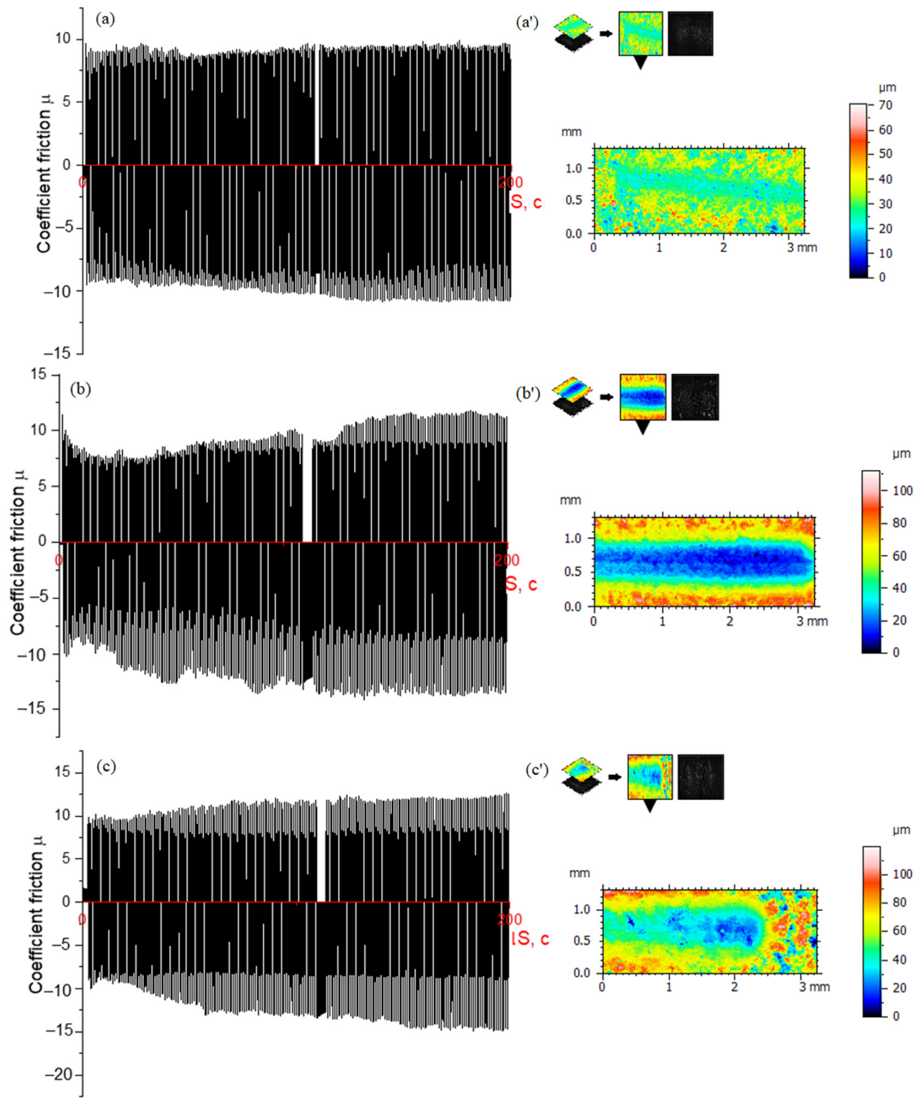

Figure 12. Dependences of the friction coefficient on the number of cycles: (**a**) TiN(34_250); (**b**) TiN(37_350); (**c**) TiN(40_450); (**a′**) TiN(34_250); (**b′**) TiN(37_350); (**c′**) TiN(34_450).

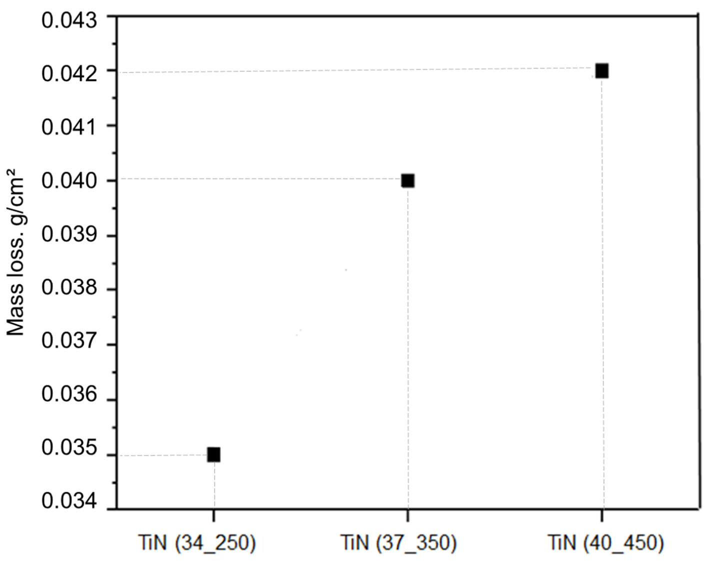

Figure 13. Mass loss results.

4. Conclusions

In this paper, the influence of PS regimes on the structure, phase composition, hardness, adhesion strength, and tribological properties of TiN coatings was studied. In the process of PS, the current strength is the main parameter determining the structure-phase states and properties of coatings. Since the current depends on the thermal energy of the plasma, the rate of spraying and the degree of thermal and chemical impact on the particles of the sprayed powder. Thus, on the basis of the obtained results, the following conclusions can be drawn:

- It was established that the phase composition of the formed coatings corresponds to the phase composition of the sprayed powder. TiN is the main phase in the coatings, and there is also a small amount of titanium oxide TiO_2. This is due to the PS process, which is carried out in open air, where the atomized material can easily react with oxygen in the air;
- The structure of the coatings depends on the energy characteristics of the injection molding process. At a current of 250 A, dense and homogeneous TiN coatings were obtained. For the plasmatron operation regime at 350 A and 450 A, the powder particles acquired a high velocity and were small in the active zone of the plasmatron, respectively, and the quality of the obtained coatings was reduced. Also, an increase in the flow rate of working gas reduces the thermal energy for heating the sprayed particles. In accordance with this, a microporous structure can be formed;
- Under optimum conditions, coatings with improved antifriction properties are formed. At a current of 250 A (regime TiN(34_250)), the wear resistance coefficient for the formed coatings decreased almost 1.5 times compared to its value for regimes TiN(37_350) and TiN(340_450). An increase in current causes the formation of a porous structure of the coatings, with developed surface relief and, as a consequence, leads to deterioration of tribological properties of coatings;
- The results of the testing of coatings for adhesion strength confirmed that coatings with high adhesion strength can be obtained by the PS method. At PS, for improvement of adhesion to the substrate, the surface of AISI 304 (1.4301) steel was pretreated by plasma to the temperature of 150–250 °C at a distance of 150 mm. As a result of the substrate heating, a coating with high adhesion strength was formed.

Thus, the conducted research has shown the prospectivity and purposefulness of the application of PS technology for obtaining TiN coatings on the surface of stainless AISI 304 (1.4301) steel.

Funding: This research has been funded by the Science Committee of the Ministry of Science and Higher Education of the Republic of Kazakhstan. (Grant No. AP14972882).

Institutional Review Board Statement: Not applicable.

Informed Consent Statement: Not applicable.

Data Availability Statement: Data are contained within the article.

Conflicts of Interest: Author Aidar Kengesbekov was employed by the company PlasmaScience LLP. The author declares that the research was conducted in the absence of any commercial or financial relationships that could be construed as a potential conflict of interest.

References

1. Budilov, V.V.; Ramazanov, K.N.; Yagafarov, I.I.; Dautov, S.K.; Yansaitova, M.I. Analiz i prognoziro-vaniye ekspluatatsionnykh povrezhdeniy pokrytiy TiN pri vozdeystvii klimaticheskikh faktorov i korrozion-no-aktivnykh sred. *Nov. Materialoved. Nauka I Tekhnika* **2015**, *5*, 2. (In Russian)
2. Barvinok, V.A.; Bogdanovich, V.I. Fizicheskiye osnovy i matematicheskoye modelirovaniye protsessov vakuumnogo ionno-plazmennogo napyleniya. *M. Mashinostroyeniye* **1999**, 35–42. (In Russian)
3. Buhl, R.; Pulker, H.K.; Moll, E. TiN coatings on steel. *Thin Solid Film.* **1981**, *80*, 265–270. [CrossRef]
4. Mamaeva, A.A.; Kenzhegulov, A.K.; Panichkin, A.V. A Study of the influence of thermal treatment on hydroxyapatite coating. *Prot. Met. Phys. Chem. Surf.* **2018**, *54*, 448–452. [CrossRef]

5. Wittmer, M.; Studer, B.; Melchior, H. Electrical characteristics of TiN contacts to N silicon. *J. Appl. Phys.* **1981**, *52*, 5722–5726. [CrossRef]
6. Valkonen, E.; Karlsson, T.; Karlsson, B.; Johansson, B.O. Annual meeting of the society: SPIE stands for: Society of Photo-Optical Instrumentation Engineers. In 1981 the Societys name was defined as SPIE—The International Society for Optical Engineering. *Proc. SPIE—Int. Tech. Conf.* **1983**, *401*, 41.
7. Klushin, M.I. *Rezaniye Metallov*; Mashgiz: Moscow, Russian, 1958; p. 454.
8. Chaus, A.S.; Rudnitskiy, F.I. Vliyaniye usloviy ekspluatatsii litogo metallorezhushchego instrumenta na osobennosti yego iznashivaniya i stoykost. Chast' 1. Analiz usloviy raboty instrumentov. *Treniye I Iznos* **2007**, *28*, 449–456. (In Russian)
9. Chaus, A.S. Osobennosti iznashivaniya instrumenta iz litoy i katanoy bystrorezhushchikh staley pri frezerovanii. *Treniye I Iznos* **1999**, *20*, 388–392. (In Russian)
10. Rakhadilov, B.; Kengesbekov, A.; Zhurerova, L.; Kozhanova, R.; Sagdoldina, Z. Impact of electronic radiation on the morphology of the fine structure of the surface layer of R6M5 steel. *Machines* **2021**, *9*, 24. [CrossRef]
11. Matsevityy, V.M. *Pokrytiya Dlya Rezhushchikh Instrumentov*; Kharkov University: Kharkov, Ukraine, 1987; p. 128.
12. Tretyakov, I.P.; Vereshchaka, A.S. *Rezhushchiye Instrumenty s Iznosostoykimi Pokrytiyami*; Mashinostroenie: Moscow, Russian, 1986; p. 190.
13. Kostyuk, G.I. *Effektivnyy Rezhushchiy Instrument s Pokrytiyem i Uprochnennym Sloyem; Monogr.-Sprav./GI Kostyuk.–KH.: Nats. Aerokosm. Un-T Khark. Aviats*; Planeta: Kyiv, Ukraine, 2007; p. 633.
14. Rakhadilov, B.; Kenesbekov, A.; Skakov, M.; Miniyzov, A. Hydrogen and deuterium storage in tungsten when irradiation with Plasma beam. In Proceedings of the METAL 2018—27th International Conference on Metallurgy and Materials, Brno, Czech Republic, 23–25 May 2018; pp. 1216–1221.
15. Tarasenko, Y.P.; Tsareva, I.N.; Fodorova, Y.A.; Levanov, Y.K. Fiziko-mekhanicheskiye i korrozionnyye svoystva ionno-plazmennykh pokrytiy nitrida titana, poluchennykh pri raznykh partsial'nykh davleniyakh reaktsionnogo gaza. *Fiz. I Khimiya Obrab. Mater.* **2006**, *4*, 42–45.
16. Kenzhegulov, A.; Mamaeva, A.; Panichkin, A.; Alibekov, Z.; Kshibekova, B.; Bakhytuly, N.; Wieleba, W. Comparative study of tribological and corrosion characteristics of TiCN, TiCrCN, and TiZrCN coatings. *Coatings* **2022**, *12*, 564. [CrossRef]
17. Mamaeva, A.; Kenzhegulov, A.; Panichkin, A.; Alibekov, Z.; Wieleba, W. Effect of magnetron sputtering deposition conditions on the mechanical and tribological properties of wear-resistant titanium carbonitride coatings. *Coatings* **2022**, *12*, 193. [CrossRef]
18. Pavlov, A.; Sagdoldina, Z.; Kassymov, A.; Seitkanova, A.; Rakhadilov, B.; Kengesbekov, A. Physico-mechanical properties, structure, and phase composition of (BeO+TiO)-ceramics containing TiO nanoparticles (0.1–2.0 wt.%). *Mater. Sci.-Pol.* **2021**, *39*, 626–638. [CrossRef]
19. Sagdoldina, Z.; Rakhadilov, B.; Kurbanbekov, S.; Kozhanova, R.; Kengesbekov, A. Effect of irradiation with Si+ ions on phase transformations in Ti–Al system during thermal annealing. *Coatings* **2021**, *11*, 205. [CrossRef]
20. Vaz, F.; Ferreira, J.; Ribeiro, E.; Rebouta, L.; Lanceros-Méndez, S.; Mendes, J.A.; De Rijk, J. Influence of nitrogen content on the structural, mechanical and electrical properties of TiN thin films. *Surf. Coat. Technol.* **2005**, *191*, 317–323. [CrossRef]
21. Vaz, F.; Machado, P.; Rebouta, L.; Cerqueira, P.; Goudeau, P.; Riviere, J.P.; De Rijk, J. Mechanical characterization of reactively magnetron-sputtered TiN films. *Surf. Coat. Technol.* **2003**, *174*, 375–382. [CrossRef]
22. Bacci, T.; Bertamini, L.; Ferrari, F.; Galliano, F.P.; Galvanetto, E. Reactive Plasma Spraying of Titanium in Nitrogen Containing Plasma Gas. *Mater. Sci. Eng. A* **2000**, *283*, 189–195. [CrossRef]
23. Kobayashi, A. Formation of TiN Coatings by Gas Tunnel Type Plasma Reactive Spraying. *Surf. Coat. Technol.* **2000**, *132*, 152–157. [CrossRef]
24. Xiao, L.S.; Yan, D.R.; He, J.N.; Zhu, L.; Dong, Y.C.; Zhang, J.X.; Li, X.Z. Nanostructured TiN Coating Prepared by Reactive Plasma Spraying in Atmosphere. *Appl. Surf. Sci.* **2007**, *253*, 7535–7539. [CrossRef]
25. Zou, D.Y.; Xiao, L.; Dong, Y. Characterization of Nanostructured TiN Coatings Fabricated by Reactive Plasma Spraying. *Surf. Coat. Technol.* **2008**, *202*, 1928–1934. [CrossRef]
26. Jasinski, M.; Szuzucki, P.; Dors, M.; Mizeraczyk, J.; Lubanski, M.; Zakrzewski, Z. Decomposition of fluorohydrocarbons in atmosphericpressure flowing air using coaxial-line-based microwave torch plasma. *Czechoslov. J. Phys.* **2000**, *50*, 285–288. [CrossRef]
27. Kengesbekov, A.; Sagdoldina, Z.; Torebek, K.; Baizhan, D.; Kambarov, Y.; Yermolenko, M.; Abdulina, S.; Maulet, M. Synthesis and Formation Mechanism of Metal Oxide Compounds. *Coatings* **2022**, *12*, 1511. [CrossRef]
28. Rodero, A.; Quintero, M.C.; Sola, A.; Gamero, A. Preliminary spectroscopic experiments with helium microwave induced plasma produced in air by use of a new structure: The axial injection torch. *Spectrochim. Acta Part B* **1996**, *51*, 467–479. [CrossRef]
29. Rakhadilov, B.K.; Kurbanbekov, S.R.; Kilishkhanov, M.K.; Kenesbekov, A.B.; Amanzholov, S. Changing the structure and phasestates and the microhardness of the R6M5 steel surface layer after electrolytic-plasma nitriding. *Eurasian J. Phys. Funct. Mater.* **2018**, *2*, 259–266. [CrossRef]
30. Kengesbekov, A.; Rakhadilov, B.; Sagdoldina, Z.; Buitkenov, D.; Dosymov, Y.; Kylyshkanov, M. Improving the efficiency of air plasma spraying of titanium nitride powder. *Coatings* **2022**, *12*, 1644. [CrossRef]
31. *ASTM G99*; Test Method for Wear Testing with a Pin-on-Disk Apparatus. ASTM: West Conshohocken, PA, USA, 2017.
32. *ASTM G133*; Standard Test Method for Linearly Reciprocating Ball-on-Flat Sliding Wear. ASTM: West Conshohocken, PA, USA, 2016.

33. Kowalewski, P.; Wieleba, W.; Leśniewski, T. Stanowisko do badań tribologicznych w złożonym ruchu cyklicznym toczno-ślizgowym. *Tribologia* **2007**, *2*, 303–311.
34. *GOST 23.208-79*; Ensuring Wear Resistance of Products. Tests of Materials for Wear Resistance When Rubbing Against Non-rigidly Fixed Abrasive Particles. GostPerevod: Moscow, Russia, 1979.
35. Ma, H.; Miao, Q.; Liang, W.; Sun, S.; Qi, Y.; Jia, F.; Chang, X. Wear Behavior of TiN/TiAlSiN Nanocomposite Multilayer Coatings from Ambient Temperature to Medium Temperature. *Coatings* **2024**, *14*, 1139. [CrossRef]
36. Zheng, Q.; Li, Y.; Ma, C.; Sun, J.; Li, H.; Yue, X. Formation mechanism of the TiN containing coating on the Al_2O_3-Ti_2O_3 composite at 1400 °C nitrogen-blowing. *Ceram. Int.* **2023**, *49*, 13119–13124. [CrossRef]
37. Fan, X.J.; Song, C.; Feng, X.H.; Zhang, X.F.; Mao, J.; Deng, C.M.; Planche, M.P. A New Method of Preparing In situ Synthesized Titanium Oxide Coatings by Very Low-pressure Reactive Plasma Spraying. *J. Therm. Spray Technol.* **2022**, *31*, 1860–1868. [CrossRef]
38. Mittemeijer, E.J.; Welzel, U. The "state of the art" of the diffraction analysis of crystallite size and lattice strain. *Z. Krist.* **2008**, *223*, 552–560. [CrossRef]
39. Kobayashi, A. New applied technology of plasma heat sources. *Weld. Int.* **1990**, *4*, 276–282. [CrossRef]
40. Rickerby, D.S.; Burneet, P.J. The wear and corrosion resistance of hard PVD coatings. *Surf. Coat. Technol* **1987**, *33*, 191–211. [CrossRef]
41. Lang, F.; Yu, Z. The corrosion resistance and wear resistance of thick TiN coatings deposited by arc ion plating. *Surf. Coat. Technol.* **2001**, *145*, 80–87. [CrossRef]
42. Khrustalyov, A.; Monogenov, A.; Baigonakova, G.; Akhmadieva, A.; Marchenko, E.; Vorozhtsov, A. Effect of TiN coating on the structure, mechanical properties and fracture of the Mg-Ca-Zn alloy. *Metals* **2022**, *12*, 2140. [CrossRef]
43. Ghailane, A.; Maadane, E.Y.; Barchid, A.; Berchane, S.; Badre-Eddine, S.; Larhlimi, H.; Makha, M. Influence of annealing temperature on the microstructure and hardness of TiN coatings deposited by high-power impulse magnetron sputtering. *J. Mater. Eng. Perform.* **2022**, *31*, 5593–5601. [CrossRef]
44. Bird, R.B.; Stewart, W.E.; Lightfoot, E.N. Transport Phenomena. *Transp. Phenom.* **2006**, *1*, 45–56.
45. Duan, L.L.; Yang, G.Y.; Hao, D.C.; Huang, F.; Xing, J.; Liu, K.X. Tribological and Mechanical Properties of Nanocrystalline TiN, TiAlN, and TiSiN PVD Coatings. *Strength Mater.* **2023**, *55*, 822–833. [CrossRef]
46. Kao, W.H.; Su, Y.L.; Hsieh, Y.T. Effects of duplex nitriding and TiN coating treatment on wear resistance, corrosion resistance and biocompatibility of Ti6Al4V alloy. *J. Mater. Eng. Perform.* **2017**, *26*, 3686–3697. [CrossRef]
47. Motte, P.; Proust, M.; Torres, J.; Gobil, Y.; Morand, Y.; Palleau, J.; Juhel, M. TiN-CVD process optimization for integration with Cu-CVD. *Microelectron. Eng.* **2000**, *50*, 369–374. [CrossRef]
48. Zhou, Q.; Ou, Y.; Li, F.; Ou, C.; Xue, W.; Liao, B.; Qu, G. Friction and Wear of Hard Yet Tough TiN Coatings Deposited Using High-Power Impulse Magnetron Sputtering. *Coatings* **2024**, *14*, 598. [CrossRef]
49. Kara, L.; Özkan, D.; Barış Yağcı, M.; Sulukan, E.; Sert, Y.; Sonsuz Sert, T. Friction and wear behaviors of TiN coatings under dry and vacuum conditions. *Tribol. Trans.* **2019**, *62*, 362–373. [CrossRef]
50. Tu, R.; Jiao, J.; Jiang, M.; Yang, M.; Ji, B.; Gao, T.; Zhang, L. Effect of Gradient Multilayer Design on Tribological Performance of TiN/TiSiN Coatings Prepared by Cathodic Arc Ion Plating. *Coatings* **2023**, *13*, 836. [CrossRef]